Macrophage Cholesterol Homeostasis Underpins the Role of Sertraline as an Adjunctive Agent in Tuberculosis Therapy.

Kanika Bisht [1,2], Riya Sahu [1,2], Sneha Vasudevan [3], Simran Jit [1,2], Nikita Bhor [1,2], Jitendra Kumar [1], Mahima Madan [1,2], Deepthi Shankaran [1,2], Sherry Bhalla [1,2], Nagasuma Chandra [3], Vivek Rao [1,2]*

1-CSIR- Institute of Genomics and Integrative Biology, Mathura Road, New Delhi-110025 India.

2- Academy of Scientific and Innovative Research (AcSIR), Ghaziabad, 201002, India

3-IISc Mathematics Initiative, Indian Institute of Science, Bangalore 560012, India, Department of Biochemistry, Indian Institute of Science, Bangalore 560012, India, Centre for Biosystems Science and Engineering, Indian Institute of Science, Bangalore 560012, India

*Corresponding author: Tel: +91 11 29879229, E-mail: vivek.rao@igib.res.in.

Classification: Biological Sciences (Major), Infectious Diseases (Minor)
Key words: *Mycobacterium tuberculosis*/ host-directed therapy/ antidepressant/ sertraline

Running Title: Sterol homeostasis dictates Mtb control

Abstract:

Cellular metabolism plays a deterministic role in the macrophage responses to intracellular pathogens such as *Mycobacterium tuberculosis* (Mtb) and infection control. Here, we demonstrate that the significant rewiring of the macrophage cholesterol metabolism by sertraline (SRT), an FDA-approved antidepressant, effectively enhances bacterial control. SRT, by virtue of its potent cationic amphiphilicity leads to the accumulation of lysosomal cholesterol in macrophages and activating the transcription factor SREBP2 and enhancing cholesterol biosynthesis. By specific gene silencing and biochemical inhibition assays, we further demonstrate that this metabolic reprogramming promotes lysosomal membrane permeabilization, mitochondrial reactive oxygen species (ROS) generation, heightened IL-1β release, collectively enhancing macrophage bactericidal activity. Our results thus highlight a previously underappreciated link between

27 cholesterol homeostasis and inflammasome activation, which contributes to improved Mtb
28 clearance in the presence of adjunctive sertraline therapy.

29 **Statement of significance:**

30 Tuberculosis remains a leading cause of global mortality, and treatment success is limited due to
31 a long treatment regimen. This study identifies macrophage cholesterol homeostasis as a central
32 pathway to enhance anti-tubercular therapy. We show that Sertraline, an FDA-approved
33 antidepressant, a cationic amphiphilic drug (CAD), reprograms cholesterol trafficking through
34 NPC1 inhibition. This drives the consequential processing of the master regulator SREBP2,
35 accompanied by lysosomal membrane permeabilization. Collectively, these lead to mitochondrial
36 ROS production and activation of NLRP3 signalling, boosting inflammasome-mediated bacterial
37 clearance. By establishing cholesterol sequestration as the mechanistic basis of host-directed
38 activity of sertraline and distinguishing it from ineffective CADs, our work provides a mechanistic
39 framework for developing cholesterol-modulating host-directed adjuncts to improve TB treatment
40 outcomes.

41 **Graphical abstract: SRT induced lysosomal cholesterol accumulation results in enhanced**
42 **bacterial control via inflammasome activation**

43

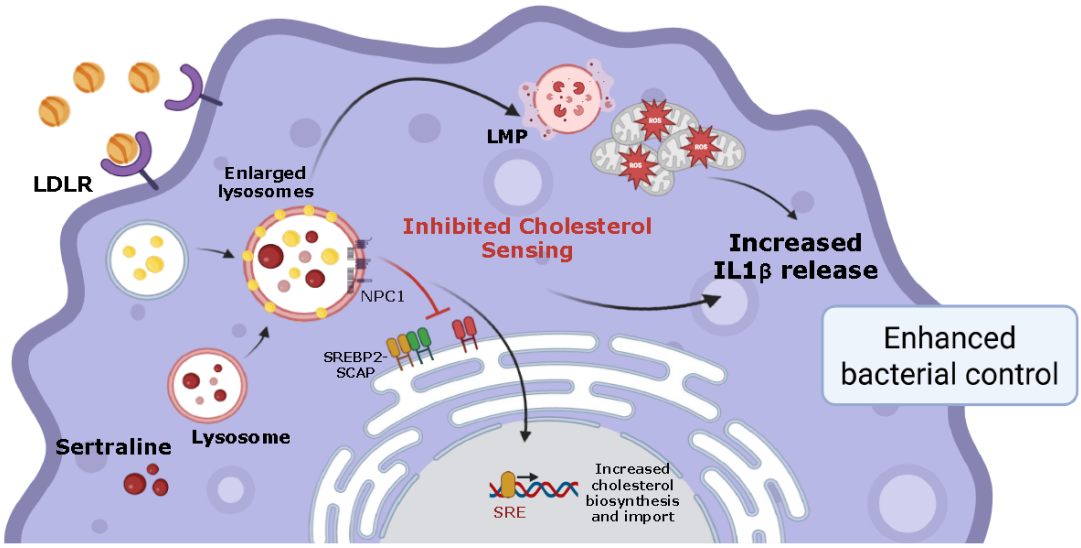

52 **Introduction:**

53 Tuberculosis (TB), caused by *Mycobacterium tuberculosis* (Mtb), remains the leading cause of
54 death from a single infectious agent globally, outpacing all other bacterial and viral pathogens (1-
55 3). The multiple initiatives to curb the infection have not been successful enough to eradicate the
56 disease, instead have led to an increase in drug resistance in the population (4, 5). These
57 limitations have spurred an interest in therapeutic strategies designed to aid the host in controlling
58 infection. Such host-directed therapies (HDTs) have relied on harnessing the cellular
59 physiological pathways to enhance antimicrobial properties (6-8). We have previously shown that
60 sertraline (SRT), a selective serotonin reuptake inhibitor (SSRI), can act as a potent adjunct to
61 standard anti-TB therapy (ATT), accelerating bacterial clearance, improving tissue resolution, and
62 enhancing host survival in preclinical infection models (9). These properties are associated with
63 the restriction of type I IFN responses via the activation of the host inflammasome pathway, thus
64 defining the therapeutic potential of manipulating host immunity for infection control (10).

65 Recent findings strongly advocate for the influence of host sterol metabolism in regulating the
66 inflammatory capacity of innate immune cells (11-13). More importantly, oxysterols have emerged
67 as promoters of the pro-inflammatory capacity of macrophages (14, 15). Recently, SREBP2, the
68 master regulator of cellular cholesterol metabolism has been associated with the direct activation
69 of the host cell inflammasomes via the NLRP3 axis (16).

70 Here, we demonstrate that the ability of SRT to adjunctively augment intracellular bacterial control
71 with frontline TB drugs is contingent on the significant alteration of macrophage cholesterol
72 homeostasis. We demonstrate that treatment with SRT leads to a significant increase in
73 intracellular cholesterol levels in Mtb-infected macrophages. We sought to investigate the
74 mechanistic basis and consequence of this increase on bacterial growth control by employing
75 chemical modulation and gene silencing, and demonstrate that the SRT induces significant
76 cholesterol buildup in the macrophage lysosomes, resulting in distinct membrane
77 permeabilization (LMP) and mitochondrial reactive oxygen species (ROS) production. We thus

78 highlight a novel connection between cellular sterol homeostasis and the inflammasome mediated
79 IL1β release in Mtb-infected macrophages. Taken together, our findings provide a strong
80 mechanistic link between the cellular metabolic machinery (cholesterol metabolism) and
81 antimicrobial efficacy. This work offers both conceptual and translational insights into leveraging
82 host metabolism as a host-directed therapeutic strategy to improve TB treatment outcomes.

83 **Results:**

84 **Treatment with sertraline increases cellular cholesterol in macrophages**

85 In an attempt to decipher the underlying mechanism for sertraline- mediated increase of antibiotic
86 efficacy in Mtb infections, global expression profiles of Mtb-infected THP1 macrophages with a
87 combination of isoniazid (H) and rifampicin (R) with (SRT) were compared with HR-treated cells.
88 A total of 160 genes of cholesterol homeostasis were differentially upregulated on treatment with
89 HRS (HR with SRT) when compared to HR treatment (Figure 1A). Interestingly, cholesterol
90 homeostasis emerged as the most significantly enhanced metabolic pathway along with an
91 increase in the mTORC1 signaling complex in macrophages treated with HRS (Figure 1B). In fact,
92 HRS-treated macrophages displayed a significant increase in the expression of genes involved
93 in cholesterol biosynthesis (Figure 1C) and import, with the markedly lower expression of sterol
94 export genes (Figure 1D). A similar pattern was reflected in SRT or HRS-treated macrophages
95 by qRT-PCR. While infection or treatment with HR failed to alter the expression of genes involved
96 in cholesterol metabolism, genes involved in biosynthesis and import were 3-5-fold higher with
97 treatment with HRS or SRT at 24 h of infection (Figure 1E). This increment in gene expression
98 reflected as an SRT-dependent 1.2-1.5-fold increase in intracellular cholesterol (Figure 1F). To
99 specifically inhibit cholesterol biosynthesis, we employed a pharmacological inhibitor of *HMGCR*,
100 simvastatin. Contrary to our expectations of diminishing antibiotic efficacy, the addition of
101 simvastatin significantly enhanced the control of Mtb by antibiotics by 3-5-fold in comparison to
102 the cells treated with HR or HRS alone (Figure 1G). Previous reports have suggested that statins,

103 in turn, can enhance expression of genes in cholesterol biosynthesis (17), we also tested for the
104 gene expression following treatment with statins. Treatment with simvastatin induced the
105 expression of the genes of the biosynthetic pathway as well as genes of cholesterol import. Also,
106 a decrease in the cholesterol export genes has been observed with simvastatin treatment (Figure
107 1H). This suggested that the increased involvement of the pathway may be crucial in enhancing
108 bacterial control by SRT.
109
110
111
112
113
114
115
116
117

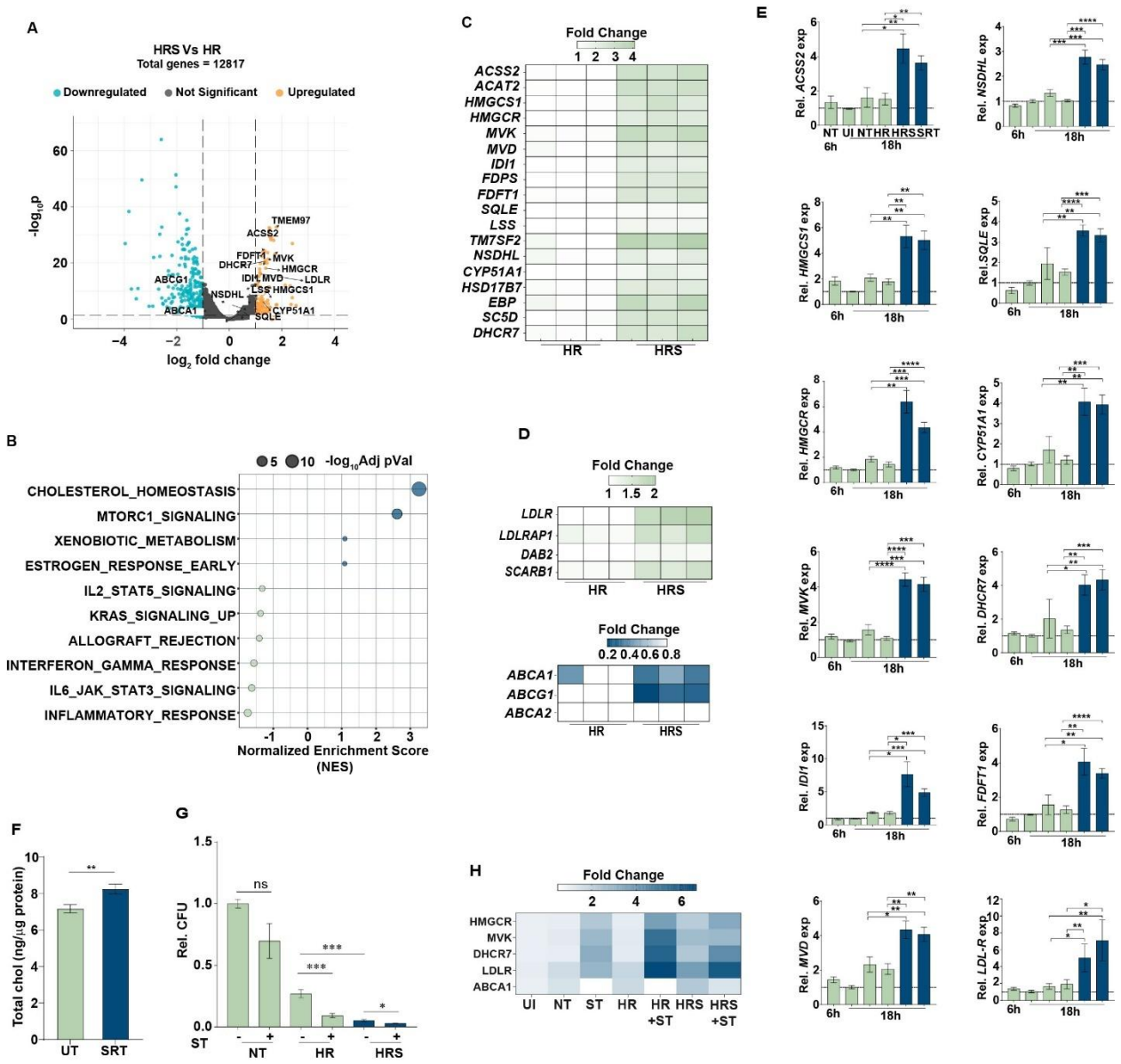

Figure 1: Global transcriptomics of Mtb-infected macrophages following treatment with sertraline.

A) A comparison of the differentially expressed genes in Mtb-infected macrophages following an 18 h treatment with HR or HRS is shown as a volcano plot. Y- and X-axes denote the $-\log_{10}$ P values and $\log_2$ fold change, respectively. The upregulated genes with ≥ 2 fold

143 change with p-value of ≤ 0.01 are highlighted in orange, while the downregulated genes
144 with ≤ -2 fold change with p-value of ≤ 0.01 are in blue.
145 B) GSEA analysis of the top significantly enriched gene sets in HRS vs HR is represented as
146 a bubble plot. Gene sets that are significantly (P-value ≤ 0.05, 0.01) enriched (Blue) or
147 downregulated (green) are represented, with the X-axis denoting the normalized
148 enrichment score.
149 C-E) Gene expression patterns in HR and HRS-treated macrophages: Expression of genes
150 involved in cholesterol biosynthesis (C) and cholesterol trafficking (D), normalised to the
151 untreated controls in the RNA-seq data was validated by gene-specific qRT-PCR (E). The
152 relative expression of specific genes relative to *GAPDH* is represented as fold change w.r.t
153 uninfected control (UI) at 6h ± SEM of triplicate assays from 3 independent experiments
154 (N=3).
155 F) Cholesterol levels in THP1 macrophages after treatment with sertraline (SRT) for 24 hours.
156 Total free cholesterol was normalized to the amount of protein and is represented as mean
157 ± SEM for triplicate assays of three independent experiments (N=3).
158 G) Growth of Mtb in HR or HRS treated macrophages that were treated with 10μM simvastatin
159 (ST) for 3 days. Bacterial numbers are represented as mean $\log_{10}$ CFU ± SEM from
160 triplicate assays of three or four independent experiments (N = 3 or 4).
161 H) Effect of simvastatin on the expression of genes for biosynthesis (HMGCR, MVK, DHCR7),
162 import (LDLR), and export (ABCA1) of cholesterol in Mtb-infected macrophages, after 18
163 h of treatment. The relative expression of specific genes, normalized to GAPDH, is
164 represented as the fold change ± SEM of triplicate assays from three independent
165 experiments (N = 3).
166 P values less than 0.05, 0.01, 0.005 are represented as *, ** and *** respectively.
167 **Lysosomal cholesterol accumulation is crucial for Mtb control in macrophages**

168 Cholesterol levels in different subcellular locations are tightly regulated to maintain a steady state
169 in cells. To test the effect of increased cellular cholesterol on intracellular distribution,
170 macrophages were stained with the cholesterol specific dye- filipin and visualized by fluorescence
171 microscopy. While filipin staining was primarily concentrated on the membranes of untreated (UT)
172 cells with minimal staining within, treatment with SRT severely impacted intracellular sterol levels,
173 with cells displaying significantly higher intracellular staining in addition to the membrane (Figure
174 2A).
175 To further identify the intracellular niche of the accumulated cholesterol, cells fed with NBD-
176 cholesterol were stained with the lysotracker that labels acidic compartments consistent with the
177 lysosomes. While in the untreated cells, minimal levels of NBD-cholesterol co-localized with
178 lysotracker, the majority of the internalized cholesterol in SRT-treated cells was found to be
179 accumulated in these compartments, indicating a pronounced accumulation of cholesterol in the
180 acidic lysotracker positive compartments corresponding to lysosomes with SRT treatment (Figure
181 2B, C).
182 In order to understand if this increase in cholesterol biosynthesis was a generic property of SSRIs,
183 another widely used antidepressant, citalopram, was tested for its ability to control intracellular
184 bacterial growth. Surprisingly, the addition of citalopram to the frontline TB drugs-HR did not affect
185 bacterial control in macrophages, unlike the increased control of infection by HRS in comparison
186 to the antibiotics alone (Figure 2D). Remarkably, unlike SRT, citalopram induced only a modest
187 and heterogeneous increase in lysosomal cholesterol accumulation, with the effect restricted to a
188 small subset of cells, and did not enhance expression of the genes involved in cholesterol
189 biosynthesis (Figure 2E, F).
190
191
192
193

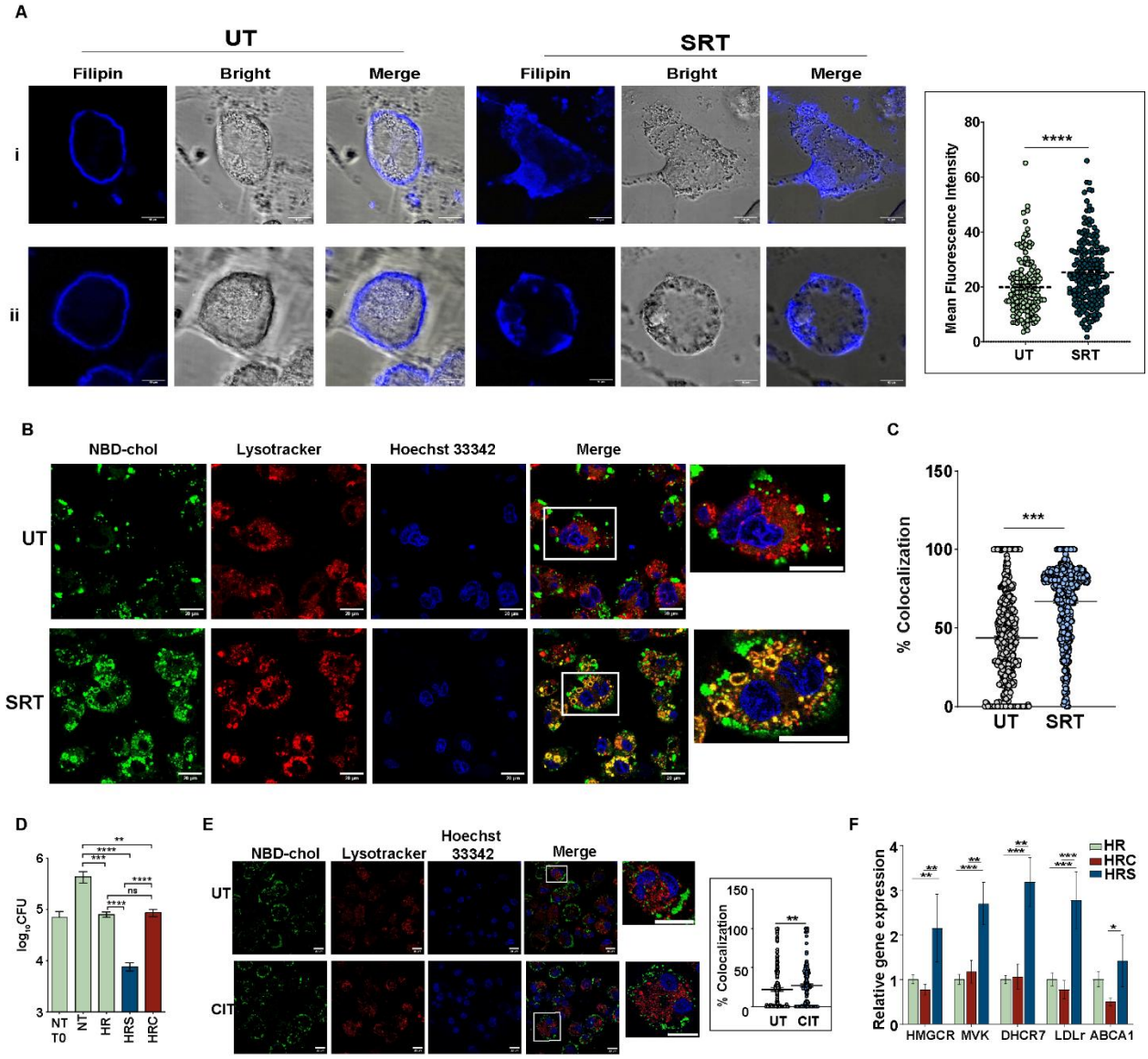

Figure 2

Figure 2: Sertraline treated macrophages accumulate lysosomal cholesterol.

A-C) Cholesterol quantitation in THP1 macrophages after SRT treatment for 24 h. A) Representative confocal images of two independent cells (i and ii) stained for cholesterol with filipin and quantitated densitometrical (box). B) Representative confocal images of cells fed with NBD-cholesterol and stained with lysotracker Red and Hoechst 33342 were imaged and quantitated for the extent of colocalization of the NBD-cholesterol and lysotracker positive

219 compartments and is depicted as mean % co-localization from multiple fields of three
220 independent experiments. Scale bar = 10μm/ 20μm.
221 D) Intracellular bacterial growth was estimated in Mtb–infected THP1 macrophages left untreated
222 (NT) or treated with (HR alone or HRC (HR in combination with 20 μM citalopram (CIT)) for 3
223 days. The data are represented as mean $\log_{10}$ values ± SEM from triplicate assays of four
224 independent experiments (N = 4).
225 E) Representative confocal images of THP1 macrophages treated with citalopram (CIT) along
226 with NBD-cholesterol for 24 hours and stained with lysotracker Red, and the colocalization
227 percentage is calculated using ImageJ. Scale bar = 20μm.
228 F) Gene expression levels in macrophages infected with Mtb, followed by treatment with HR alone
229 or with citalopram. The relative expression of the specific gene, relative to GAPDH, is represented
230 as fold change with respect to HR ± SEM of triplicate assays from three independent experiments
231 (N=3).
232 P values less than 0.05, 0.01, 0.005 are represented as *, ** and *** respectively.
233
234 **Sertraline enhances SREBP2 processing in macrophages**
235 The feedback activation of SREBP2 in response to the absence of cholesterol sensing in the ER
236 on account of lysosomal accumulation is well documented (18, 19). To assess whether SRT
237 activates the signaling cascade, levels of mature SREBP2 (mSREBP2) were measured in
238 macrophages following SRT treatment. Indeed, commensurate with the significant induction of
239 the SREBF2 gene in HRS-treated macrophages, in both the global transcriptomic data and with
240 qRT-PCR analysis, macrophages treated with SRT harbored ~2-fold higher levels of the cleaved,
241 active form of SREBP2 (mSREBP2) by 24h compared to the untreated cells (Figure 3A-D). The
242 relatively unchanged levels of mSREBP2 in both untreated and citalopram treated cells, lend
243 further support to the importance of this signaling axis in the antibiotic potentiating effect of SRT
244 (Figure 3 E, F).

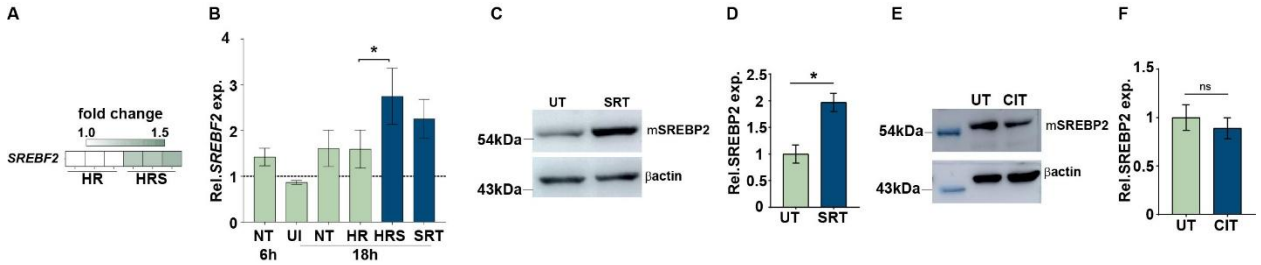

Figure 3

Figure 3: Sertraline enhances SREBP2 processing in macrophages.

A -B) Expression levels of *SREB*F2 in the global transcriptomic analysis dataset (A) or quantified by qRT-PCR (B) in Mtb-infected macrophages left untreated (NT) or treated with HR, HRS, or SRT for 18h. The relative expression of specific genes relative to *GAPDH* is represented as fold change ± SEM of triplicate assays of three independent experiments (N=3).

C-F) The levels of SREBP2 in protein extracts of macrophages left untreated, treated with SRT (C) or 20μM of citalopram (E) for 24 hours were checked by immunoblotting with specific antibodies for SREBP2 and β-actin and quantified by densitometry (D, F). The reactivity for SREBF2 in cells relative to β-actin was quantified in three independent experiments (N=3) and is represented as mean ± SEM.

P values less than 0.05, 0.01 and 0.005 are represented as *, ** and *** respectively.

SREBP2 processing is critical for controlling intracellular Mtb growth:

SREBP2 activation is regulated by multiple feedback mechanisms; typically, cholesterol and oxysterols have been shown to downregulate this process by modulating the SCAP-SREBP2 egress to the Golgi (20). To test the importance of SREBP2 activation on Mtb control, macrophages were treated with cholesterol exogenously to inhibit SREBP2 processing and tested for their ability to control Mtb growth in the presence of HR or HRS. Addition of cholesterol significantly inhibited SREBP2 processing (2-fold) (Figure 4A, Figure S1A) and resulted in a significant reversal (5-fold) of the effect of SRT on antibiotic potentiation (Figure 4B). Further, the

271 inhibition of SREBP2 activation with a specific S2P protease inhibitor- 1,10-phenanthroline,
272 resulted in a partial but significant reversal of bacterial control by SRT (3-4-fold higher bacterial
273 numbers than HRS alone) (Figure 4C). To further test the relevance of SREBP2 processing,
274 macrophages deficient in the SREBP2 cleavage activation protein (SCAP) were tested for their
275 ability to restrict Mtb growth. As expected, THP1 cells with >50% silencing of *SCAP* with specific
276 shRNAs displayed significantly lower levels of mature SREBP2 in comparison to the cells treated
277 with scrambled shRNAs (SCR) (Figure 4D-F). Consistent with the inhibition of S2P, silencing of
278 SCAP reduced the effectiveness of SRT on Mtb control without affecting the uptake of bacteria
279 (Figure 4G). As observed in Figure 4G, SCAP-silenced macrophages harbored significantly 3-4-
280 fold higher bacterial numbers than the control cells. Even in the untreated cells, loss of SCAP
281 severely impaired the ability to control Mtb with nearly 3-fold higher CFU in the SCAP-deficient
282 cells than in the control (Inset, Figure 4H), corroborating the requirement of SREBP2 maturation
283 in
284 Mtb

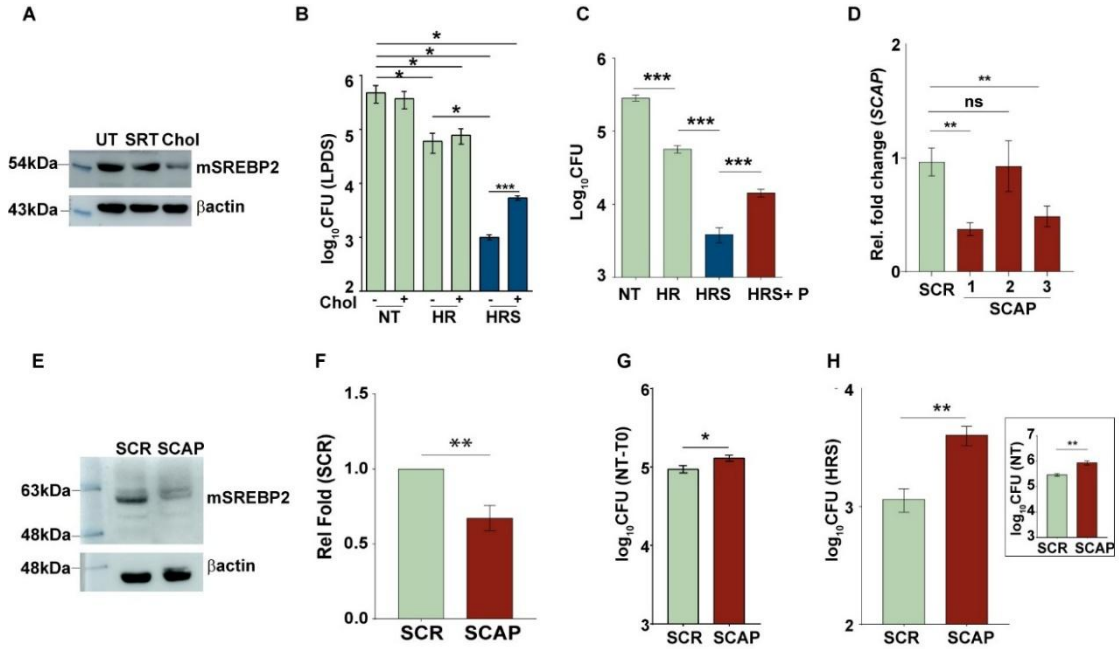

Figure 4

285 control by macrophages.

286

287

288 **Figure 4: SREBP2 processing is critical for controlling intracellular Mtb growth.**

289 A) The levels of SREBP2 in cell extracts of macrophages treated with 20µg/ml of cholesterol
290 for 24 h were analysed by immunoblotting. The levels of β-actin were used as the control
291 values for the comparison.

292 B-C) The intracellular bacterial growth was estimated in Mtb-infected macrophages that were
293 either untreated or treated with (B) cholesterol or (C)- 0.5 mM of 1,10-phenanthroline (P)
294 for 1 hour. This was followed by treatment with HR and HRS alone, in combination with
295 cholesterol, which was replenished every 24 hours in the LPDS media, or with 1,10-
296 phenanthroline. The data is represented as mean $\log_{10}$ values ± SEM from triplicate
297 assays of four independent experiments (N = 4).

298 (D) Evaluation of gene expression levels in *SCAP-silenced* macrophages. The relative
299 expression of the *SCAP* is represented as fold change ± SEM w.r.t. scrambled control in
300 triplicate assays from three independent experiments (N=3).

301 (E) Estimation of mature SREBP2 in protein extracts of *SCAP-silenced* cells by immunoblotting
302 with specific antibodies for SREBP2 and β-actin. The protein marker used is Prestained
303 Protein ladder (MBT092).

304 (F) Densitometric quantification of the reactivity for SREBP2 in cells relative to β-actin of six
305 independent experiments (N=6) is represented as mean ± SEM.

306 (G) Bacterial uptake in *SCAP-silenced* cells compared to scrambled control after 6 hours of
307 incubation with Mtb at MOI 5.

308 (H) Intracellular growth of Mtb is depicted in untreated (NT) (inset) or HRS-treated *SCAP-*
309 *silenced* cells. The data are represented as mean $\log_{10}$ values ± SEM from triplicate
310 assays of three independent experiments (N = 3).

311

312 **SRT recapitulates key features of NPC1 inhibition in macrophages.**

313 A similar phenotype of organellar sterol accumulation, specifically in the endosomal-lysosomal
314 compartments, is a characteristic feature of NPC1 mutation/ deficiency in the human population
315 (21, 22). A strong binding of SRT and the related antidepressant – indatraline, with the N-terminal
316 domain of NPC-1, has been shown to cause accumulation of cholesterol in lysosomes (23). In
317 order to investigate the relevance of this mechanism, a computational structural analysis using
318 ligand docking for SRT with NPC-1 was performed. The well-established cargo for NPC1-
319 cholesterol, resulted in the identification of a prominent cluster of docked poses with 88% of the
320 docked poses and a mean binding energy of -10.68 kcal/mol (Figure 5A). Having established the
321 correct binding pose, the binding of SRT was tested. Docking of sertraline in the same framework
322 indicated that the docked poses clustered into 2 prominent different clusters, with the top-ranked
323 cluster comprising 56% of the poses, a mean binding energy of -8.28 and -8.13 kcal/mol (Figure
324 5B). Similar to cholesterol, SRT is also stabilized by hydrophobic interactions and hydrogen
325 bonds, forming a stable protein-ligand complex with a defined pose, indicating its ability to bind to
326 NPC1.
327 Given its inability to impact lysosomal cholesterol distribution, the other SSRI, citalopram, was
328 evaluated for its ability to bind to NPC-1. In contrast to cholesterol and SRT, the docked poses
329 were found to be distributed across six different clusters, with the top-ranked cluster comprising
330 32% of the docked poses (mean binding energy = -7.67 kcal/mol), indicating the absence of a
331 defined pose for citalopram in the NPC1 site, suggestive of poor binding to NPC-1 (Figure 5C).
332 To test the relevance of this binding on bacterial control, the specific inhibitor, U18666A, was
333 tested for its NPC-1 binding capacity and the ability to enhance antibiotic efficacy in macrophages.
334 Surprisingly, U18666A also bound specifically to the same binding pocket as cholesterol with a
335 prominent cluster comprising 92% of the docked poses, having a mean binding energy of -9.66
336 kcal/mol (Figure 5D) (Interactions listed in Suppl table S1). The binding energies computed for
337 the best docked poses of the ligands, cholesterol, and U18666A indicate high affinities in both
338 cases (binding energies -10.82 kcal/mol and -9.71 kcal/mol, respectively), possibly due to the

339 stabilization by a large number of hydrophobic interactions. While the best docked poses of SRT
340 also indicated a high affinity (binding energy –8.31 kcal/mol), citalopram bound NPC1 at a lower
341 affinity of -7.88 kcal/mol (Figure 5E).
342
343 In addition, Citalopram had a higher torsional penalty than SRT, lending it a poorer ligand to NPC1
344 as compared to sertraline (Figure 5F). Further analysis of cholesterol levels in U18666A-treated
345 macrophages revealed a pronounced accumulation in the lysotracker positive compartments with
346 the consequent SREBP2 processing and activation, with an enhanced expression of the
347 cholesterol biosynthetic machinery similar to SRT (Figure 5G, H, S1B). To verify the importance
348 of increased SREBP2 processing in Mtb control, the effect of antibiotics was tested in cells treated
349 with U18666A. Addition of U18666A to the frontline TB drugs -HR resulted in a 3-4-fold better
350 control of Mtb in macrophages by day 3 of infection, emphasizing the relevance of lysosomal
351 cholesterol loading in bacterial control (Figure 5I). To simulate conditions of enhanced cholesterol
352 biosynthesis via increased SREBP2 activation, we resorted to silencing INSIG1, the inhibitor of
353 SCAP-SREBP2 translocation for processing and activation at the Golgi, and observed a
354 significant (>60%) decrease in the levels of INSIG1 expression (Figure 5J). However, we did not
355 observe any detectable change in the levels of mature SREBP2 in these macrophages (Figure
356 S1C). As an alternative, macrophages were treated with brefeldin A (BFA) to facilitate constitutive
357 proteolysis and activation of SREBP2 due to the collapse of the ER-Golgi network(24). In sync
358 with our expectations, the addition of BFA significantly increased the expression of active
359 SREBP2 in macrophages (2-fold- Figure 5K, Figure S1D) that reflected as a 3-4-fold decrease in
360 bacterial numbers in HR treated cells, further emphasizing the importance of SRT-mediated
361 increase in SREBP2 activation in the ability of macrophages to restrict bacteria (Figure 5L).

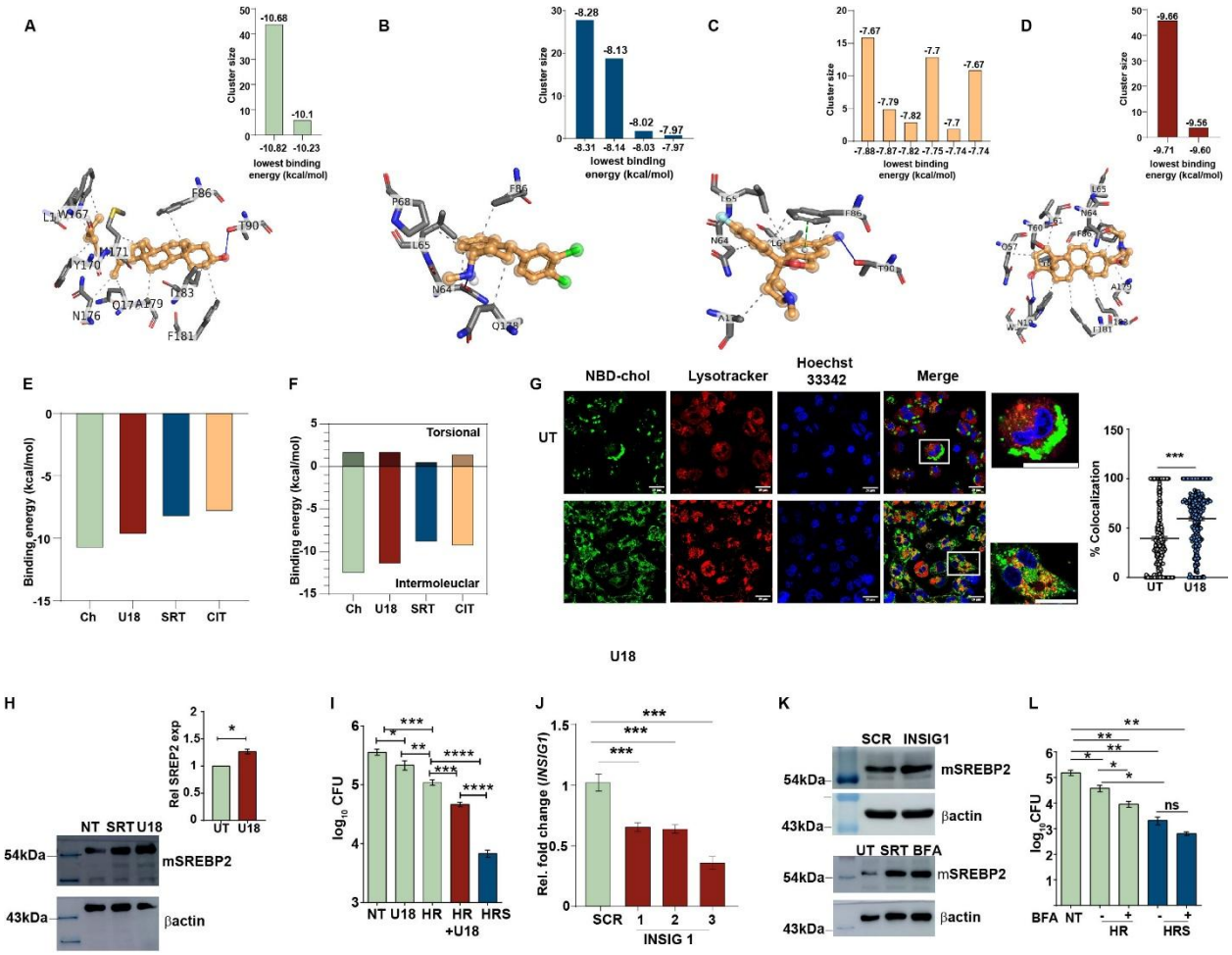

Figure 5

Figure 5: SRT treatment phenocopies NPC1 deficiency.

A-D) The best docked poses for Cholesterol (A), Sertraline (B), Citalopram (C), and U18666A (D), having the lowest binding energy. Bar plots represent the clusters of docked poses and binding sites (Mean binding energy (kcal/mol) for each cluster is mentioned at the top of the bar). Grey dotted line: hydrophobic interactions, blue solid line: hydrogen bonds, green dotted line: pi-pi stacking.

E-F) The bar plots represent the overall binding energy of each ligand (E), and (F) shows the breakdown of the overall binding energy into intermolecular energy and torsional penalty components.

387 G) The localization of cholesterol was analyzed in cells treated with 2.5 μg/ml of the NPC1
388 inhibitor- U18666A (U18). The extent of colocalization of NBD-cholesterol and lysosomes
389 (lysotracker) in macrophages was quantified and is expressed as percent co-localization from
390 three independent experiments (N=3) (inset). Scale bar = 20μm.
391 H) The extent of mature SREBP2 was evaluated in macrophages left untreated or treated with
392 U18666A by immunoblotting and densitometric analysis of the lysates. Levels of β-actin
393 expression were used as the control. The relative levels of mSREBP2 in SRT-treated cells (w.r.t.
394 untreated) are represented as relative mean expression ± SEM from six independent
395 experiments, as shown in the box (N=6).
396 I) Growth of Mtb in macrophages that were left untreated or treated with HR alone or in combination
397 with U18666A and HRS for 3 days. The CFU numbers are represented as mean $\log_{10}$ values ±
398 SEM from triplicate assays of four independent experiments (N = 4).
399 J) Expression of *INSIG1* gene was quantified by qRT-PCR. *GAPDH* expression values were used
400 as controls for normalization. The relative expression in the *INSIG1* silenced cells was compared
401 with the scrambled control and is represented as Rel. fold change mean ± SEM of triplicate assays
402 from three independent experiments (N=3).
403 K) The levels of mature SREBP2 or β- actin were analyzed by specific immunoblotting of the
404 protein lysates from *INSIG1-silenced* macrophages (Upper panel) and in THP1 macrophages left
405 untreated or treated with 3μg/ml BFA (Lower panel). Levels of β-actin expression were used as
406 the control.
407 L) Growth of Mtb in macrophages left untreated or treated with HR, HRS alone, or in combination
408 with brefeldin A (BFA) for 3 days. The CFU numbers are represented as mean $\log_{10}$ values ± SEM
409 from triplicate assays of three independent experiments (N = 3).
410 P values less than 0.05, 0.01, and 0.005 are represented as *, ** and ***, respectively.
411

412 **Loss of lysosomal integrity couples SRT-mediated cholesterol accumulation with**
413 **activation of inflammasomes.**
414 Accumulation of cholesterol in lysosomes has been associated with a significant damage to the
415 lysosomal membrane, resulting in the formation of pores, a process called lysosomal membrane
416 permeabilization (LMP) (23, 25). This loss of membrane integrity is rapidly repaired by the
417 recruitment of the ESCRT complex via the lectin-galectin 3 (26). Treatment with SRT significantly
418 induced the expression of *LGALS3* in Mtb infected macrophages (Figure 6A-B). To check if SRT
419 compromised the membrane integrity of lysosomes, cells expressing GFP-tagged galectin 3 were
420 treated with
421 SRT. As observed in Figure 6C, galectin3 was distributed uniformly in the untreated cells, in
422 contrast to the punctate signal in the cells treated with LLOme, a dipeptide documented to induce
423 lysosomal damage (27). Interestingly, SRT- treated cells also displayed punctate signals, unlike
424 the treatment with citalopram (Figure 6D), suggestive of extensive lysosomal damage. A close
425 connect between the host lysosomal cholesterol levels and mitochondrial function has been
426 established (28-30). Accumulation of cholesterol in the lysosomes has been associated with
427 altered
428 mitochondrial physiology, exacerbated ROS production, and disorders (31-34). Given our
429 previous observation for an important role for inflammasome activation by SRT (9) via the
430 induction of mitochondrial ROS (10) and an elegant study by Guo et.al, 2018, establishing a direct
431 link between the activation of SREBP2 and inflammasome induction (35), the role of cholesterol
432 accumulation by SRT as a putative cause of inflammasome activation was evaluated in Mtb
433 infections. In line with our previous studies, while SRT induces significant ROS, citalopram failed
434 to activate mitochondrial ROS in macrophages (Figure 6E-G). A direct link between the host cell
435 cholesterol accumulation, increased SREBP2 processing, and inflammasome activity was probed
436 in cells by estimating the levels of IL1β secretion in the different macrophages. Inhibition of SRT-
437 mediated SREBP2 maturation in SCAP-deficient cells reduced the secreted IL1β levels (Figure

6H). This study firmly establishes the importance of the affinity of cationic amphiphilic drugs to the NPC1 protein in augmenting bacterial control, thereby providing a novel target for the future development of host-directed therapy against infections.

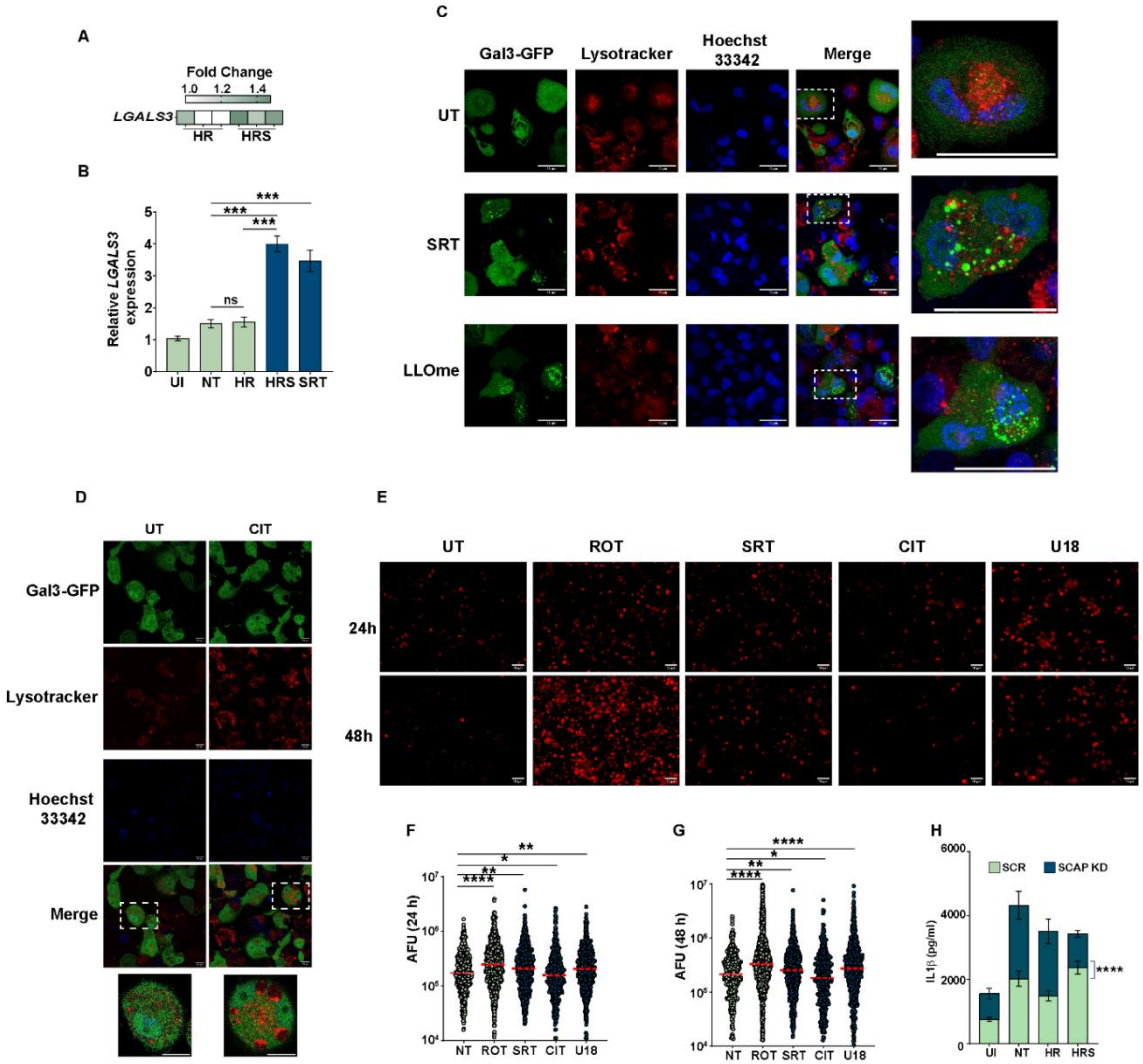

Figure 6

Figure 6: SRT-induced lysosomal cholesterol accumulation induces macrophage inflammasome

478 (A-B) Gene expression of *LGALS3* (A) in the transcriptomics data and quantified by qRT-PCR (B)
479 in the Mtb-infected macrophages after 18 hours of treatment with HR, HRS, and SRT. The relative
480 expression of specific genes relative to *GAPDH* is represented as fold change ± SEM of triplicate
481 assays of three independent experiments (N=3).
482 (C) Representative images of macrophages overexpressing GFP-tagged galectin 3 protein
483 treated with SRT for 24 hours or LLOme for 15 min and stained with lysotracker Red. Boxes
484 indicate insets, magnified on the right. Scale bar = 10μm.
485 (D) Images after citalopram treatment for 24h in GFP-tagged galectin3 overexpressing
486 macrophages. The inset represents the zoom-in. Scale bar = 10μm.
487 (E-G) Representative images showing mitoSox staining after treatment with sertraline (SRT),
488 citalopram (CIT), U18666A (U18), and rotenone (ROT) as the positive control for mitochondrial
489 ROS induction. The extent of ROS was quantified after 24 h (F) and 48 h (G) of treatment and is
490 represented as arbitrary fluorescence units (AFU) from ~ 800 cells of three independent
491 experiments (N=3).
492 (H) IL-1β levels in the supernatants of Mtb-infected SCR and *SCAP-silenced* cells following
493 treatment with HR or HRS, compared to the untreated group.
494 P values less than 0.05, 0.01 and 0.005 are represented as *, ** and *** respectively.
495
496 **Discussion:**
497 Infection control by innate immune cells is a complex process with the involvement of multiple
498 modalities, intertwining metabolic and inflammatory response pathways to ensure pathogen
499 removal (36, 37). The complexity only increases with the pathogen adept at modifying signaling
500 cascades and occupying intracellular niches that are designed for infection control (38, 39). The
501 incidence of TB, particularly, has been strongly associated with severe malnutrition(38, 39).
502 Epidemiological data suggest a strong inverse correlation between serum cholesterol levels and
503 TB incidence and mortality, with TB patients displaying severe hypocholesterolemia (40-42). In

504 fact, the enhanced levels of sputum sterilization in a small set of pulmonary TB patients on a
505 cholesterol-rich diet only highlight the importance of improving sterol levels for improved treatment
506 outcomes(43). Recent studies have also implicated a significant role of cholesterol and its
507 derivatives in dictating macrophage response dynamics (44, 45). In line with these observations,
508 we identified an important role for the host cell cholesterol metabolic pathway in the antibiotic-
509 mediated potentiation of Mtb control by SRT.
510 In this context, we demonstrate that SRT treatment enhances macrophage cholesterol
511 biosynthesis programs through robust activation of the SREBP2 processing, leading to elevated
512 intracellular cholesterol. We reasoned that altering the cholesterol biosynthetic pathway in
513 macrophages would modulate the effects of sertraline. To our surprise, sertraline activity
514 remained unaltered even in conditions of restricted biosynthesis via statins (46). Contrary to our
515 expectations, SRT treatment in the presence of statins increased the expression of the cholesterol
516 biosynthetic genes in macrophages, resulting in enhanced effect of antibiotics in controlling
517 infection, implying the compensatory activation of alternative pathways to maintain homeostasis
518 of cholesterol in cells. Notably, the SREBP2 axis emerged as a critical focal point connecting
519 cholesterol metabolism and infection control in macrophages. In concordance with recent studies
520 that suggest a direct role for statins, we also observed significant activation of SREBP2 with SRT
521 treatment in macrophages is consistent with increased bacterial control (47-49). However, both
522 genetic perturbation (silencing *SCAP*) and pharmacological activation (BFA), but not silencing of
523 *INSIG1* (induced by SRT in macrophages), confirmed the essential role of this pathway in SRT-
524 mediated Mtb restriction.
525 Our data relates the altered cholesterol trafficking and storage as vital mediators of SRT function.
526 Recently, TMEM97, a cholesterol-responsive NPC1-binding protein, has been implicated in
527 cholesterol trafficking between lysosomes and ER; RNA-interference mediated restraint of
528 TMEM97 reduces lysosomal lipid storage and restores cholesterol levels in the ER in cell models
529 of NPC1 (50). SRT-treated macrophages with increased expression of TMEM97 (Data not shown)

530 resonate with phenotypes of Niemann-Pick type C disease, with cholesterol-laden lysosomes and
531 disrupted ER-lysosome crosstalk. Along similar lines, treatment with the potent NPC1 inhibitor
532 U18666A induced significant dysregulation of cholesterol trafficking from lysosomes to the
533 endoplasmic reticulum (ER). Consistent with this, cells treated with either SRT or U18666A but
534 not with citalopram exhibited markedly enlarged lysosomes, indicative of cholesterol
535 accumulation.

536 This lysosomal sequestration appears to be a key trigger for downstream immune responses.
537 Oxysterols, particularly 25-hydroxy cholesterol (25HC), a dominant negative regulator of
538 cholesterol biosynthesis (51)acts as a dampener of inflammation, preventing the overstimulation
539 of macrophages by downregulating cholesterol biosynthesis and SREBP2 processing, in addition
540 to activating the esterification of excess free cholesterol (52, 53). 25HC is documented to protect
541 macrophages against mitochondria induced NLRP3 inflammasome activation with ch25h$^{-/-}$
542 macrophages the gene encoding for 25HC, elaborating significantly high levels of IL1β in
543 response to LPS stimulation (54, 55). Mitochondrial ROS, SCAP-SREBP2, and the *FASN*
544 effectively mediate NLRP3-mediated inflammasome activation in cells (35, 56, 57). Reduced
545 expression of *CH25H* (2-fold) and upregulation of *FASN* (~ 3-fold) suggest a coordinated
546 suppression of anti-inflammatory oxysterol signaling and a shift towards an activated inflammatory
547 state. This metabolic-inflammatory axis distinguishes SRT from related SSRIs such as citalopram,
548 which lacks these effects. In contrast, citalopram had an insignificant effect on these processes,
549 thereby validating the critical role of host cell cholesterol metabolism in macrophage-mediated
550 control of Mtb. These findings further support a model in which host cell cholesterol metabolism
551 plays a critical role in regulating mitochondrial stress and inflammasome activation, thereby
552 contributing to macrophage-mediated control of Mtb.

553 Further, the observed increase in assembly of galectin 3 close to the lysosomes in SRT-treated
554 macrophages advocates for extensive lysosomal membrane permeabilization (LMP) as a result
555 of lysosomal cholesterol accumulation, which is a property of lysosomotrophic molecules like

556 cationic amphiphilic drugs (CADs) (58). While similar effects were observed with SRT and
557 U18666A, with strong experimental evidence as a CAD, citalopram, a less well-documented
558 cationic amphiphile, failed to bind to NPC-1 protein directly to induce cholesterol accumulation
559 and resultant LMP.

560 Our findings advance a previously understudied axis of reprogramming macrophage cholesterol
561 metabolism and the consequent induction of a lysosomal stress response that enhances
562 inflammasome activation and bacterial clearance (as seen with SRT). While we effectively
563 establish a direct correlation between the induced LMP and the subsequent activation of
564 mitochondrial ROS, in line with previous reports (59, 60), a detailed analysis of the molecular
565 mechanism by which SRT and U18666A mediates LMP-induced mitochondrial ROS activation
566 will be part of a comprehensive future manuscript. While one can envisage a possible contribution
567 also of accumulated cholesterol in altering the intracellular distribution of frontline TB drugs,
568 leading to enhanced bacterial control, these will be part of future work and communications.

569 Our current findings thus emphasize the significance of evaluating host metabolic programs for
570 the design of future adjunct therapies for infection control, specifically in the population cohorts
571 with malnutrition and dyslipidemia. Taken together, our work integrates lipid metabolism and
572 innate immune signaling and places host cholesterol metabolism as a crucial determinant of TB
573 pathogenesis and treatment outcome.

574 **Author contribution**

575 KB and VR were instrumental in the design of the work. KB, RS, NB, JK, MM, and DS were
576 involved in the conduct of the work. SJ and SB were involved in the analysis of the transcriptome
577 high throughput data. None of the authors have any conflict of interest.

578 **Acknowledgements**

579 The authors thank CSIR (VR- MLP2106) for supporting the study. CSIR-STS0016 is
580 acknowledged for continuous maintenance of BSL3 and ABSL2 facilities. CSIR- BSC0403 is duly
581 acknowledge for the microscopy facility. The student fellowships from CSIR- India (KB) are

acknowledged. Biorender.com is duly acknowledged for the graphical abstract preparation. The authors thank Ms. Garima Maurya and Mr. Lakshay Kumar for proofreading and suggestions on improving the manuscript. The authors thank Dr. Michael Glickman for the LPDS media.

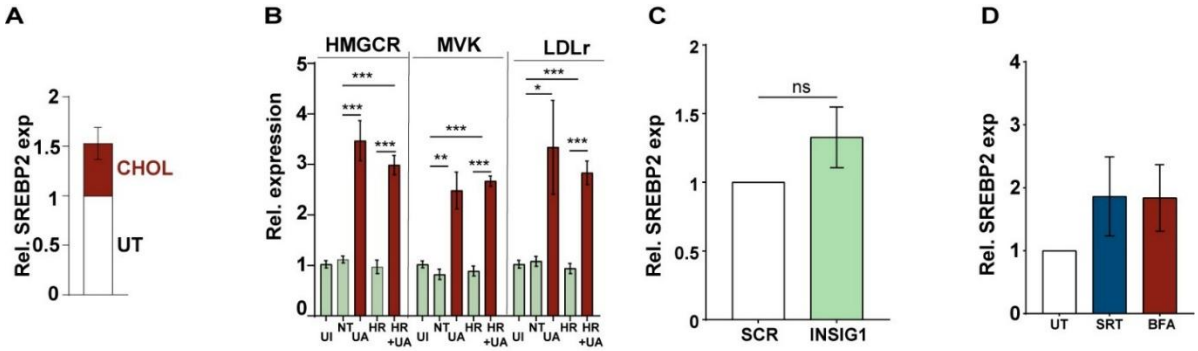

Figure S1

A) The extent of SREBP2 activation was evaluated in macrophages left untreated or treated with cholesterol for 24h by immunoblotting and densitometric analysis of the lysates. Levels of β- actin expression were used as the control. The relative levels of mSREBP2 in cholesterol-treated cells (w.r.t. untreated) are represented as relative mean expression ± SEM from three independent experiments, is shown in the box (N=3).

B) Expression of genes for cholesterol biosynthesis was quantified by qRT-PCR in the Mtb-infected macrophages left untreated or after 18 hours of treatment with HR with and without U8666A (UA). The relative expression of specific genes relative to GAPDH is represented as fold change + SEM of triplicate assays of three independent experiments (N=3).

C, D) The extent of SREBP2 activation was evaluated in SCR or *INSIG1-silenced* macrophages (C) or left untreated or treated with 3μg/ml brefeldin A (D) for 24h by immunoblotting and densitometric analysis of the lysates. Levels of β-actin expression were used as the control. The relative levels of mSREBP2 in cells (w.r.t. untreated) are represented as relative mean expression ± SEM from three independent experiments, as shown in the box (N=3).

608
609
610
611
612 **Table S1 : Binding interactions predicted for the best docked poses of each ligand**
613

Cholesterol		
Amino acid	**Ligand atom**	**Distance in Å**
Hydrophobic interactions		
PHE86	C19	3.73
L154	C25	3.64
W167	C27	3.68
Y170	C24	3.98
M171	C18	3.35
N176	C21	3.67
Q178	C21	3.51
A179	C12	3.18
F181	C2	3.95
I183	C2	3.33
Hydrogen bonds		
T90	O1	2.80
U18666A		
Amino acid	**Ligand atom**	**Distance in Å**
Hydrophobic interactions		
W5	C13	3.86
Q57	C16	3.16
T60	C16	3.54

L61	C15	3.51
N64	C23	3.88
L65	C23	3.77
F86	C23	3.48
F86	C3	3.34
F86	C7	3.59
T90	C11	3.37
A179	C25	3.99
F181	C14	3.91
I183	C6	3.27
Hydrogen bonds		
N19	O2	1.86
Sertraline		
Amino acid	**Ligand atom**	**Distance in Å**
Hydrophobic interactions		
N64	C8	3.73
L65	C8	3.13
P68	C9	3.26
F86	C7	3.08
Q178	C3	3.74
Hydrogen bonds		
A64	N11	1.99
Citalopram		

Amino acid	**Ligand atom**	**Distance in Å**
Hydrophobic interactions		
L61	C17	3.30
N64	C15	3.85
L65	C13	3.81
F86	C18	3.23
F86	C10	3.56
F86	C15	3.34
A179	C09	3.52
Hydrogen bonds		
T90	N04	2.35
pi-pi stacking		
F86		3.95

614

615 **KEY RESOURCE TABLE**

REAGENT or RESOURCE	SOURCE	IDENTIFIER
Antibodies		
Rabbit polyclonal anti- SREBP2	Invitrogen	Cat# PA1-338
Mouse monoclonal anti-β-actin	Santa Cruz biotechnology	Cat#sc-47778
Bacterial and virus strains		

Mtb Erdman strain	Animal passaged strain EF2	NA
Chemicals, peptides, and recombinant proteins		
HiGlutaXL-RPMI-1640	Himedia	Cat# AL060G
DMEM high glucose	Himedia	Cat# AL007A
Sodium pyruvate	Himedia	Cat# TCL015
Fetal bovine serum	Himedia	Cat# RM9955
Fetal bovine serum lipid depleted	Biowest	Cat# S180L
Phorbol 12-Mysristate 13-acetate(PMA)	SIGMA	Cat# P8139
Ethambutol dihydrochloride	SIGMA	Cat# E4630
Isoniazid	SIGMA	Cat# I3377
Rifampicin	Himedia	Cat# CMS1889
Pyrazinamide carboxamide	SIGMA	Cat# P7136
Sertraline	SIGMA	Cat# S6319
Citalopram hydrobromide	SIGMA	Cat#C7861
U18666A	SIGMA	Cat#U3633
Simvastatin	SIGMA	Cat#S6196
Cholesterol	SIGMA	Cat#C3045
1,10 Phenanthroline	SIGMA	Cat#131377
Brefeldin A	Invitrogen	Cat#00450651
NBD- cholesterol	Avanti	Cat# 810250P
LysoTracker Red DND-99	Invitrogen	Cat#L7528
Hoechst 33342	Gift	NA

Filipin III readymade solution	SIGMA	Cat# SAE0087
Rotenone	SIGMA	Cat# R8875
MitoSox dye	Thermo Fisher Scientific	Cat# M36008
Lipofectamine LTX reagent with Plus reagent	Thermo Fisher Scientific	Cat# 15338100
Puromycin dihydrochloride	Himedia	Cat# TC198
Cholroform EMPARTA grade	Merck	Cat# 1.07024.2500
Methanol HPLC grade	Merck	Cat# 60600725001730
16% methanol free formaldehyde	Thermo Fisher Scientific	Cat# 28908
Critical commercial assays		
BCA protein estimation kit	GBiosciences	Cat#786-571
Total cholesterol	Abcam	Cat#ab282928
Human IL-1β ELISA kit	BD	Cat#557953
ECL Western Blotting Substrate	Promega	Cat#W1015
Deposited data		

RNA sequencing	GEO database	GSE308209
Experimental models: Cell lines		
THP1/NT shRNA	This study	N/A
THP1/SCAP shRNA#1	This study	N/A
THP1/SCAP shRNA#2	This study	N/A
THP1/SCAP shRNA#3	This study	N/A
THP1/Insig1 shRNA#1	This study	N/A
THP1/Insig1 shRNA#2	This study	N/A
THP1/Insig1 shRNA#3	This study	N/A
THP1/GFP-tagged Gal3 overexpression	This study	N/A
Oligonucleotides		
Human *GAPDH* primer forward: 5'-GAAGGTGAAGGTCGGAGTC-3'	This study	N/A
Human *GAPDH* primer reverse: 5'-GAAGATGGTGATGGGATTTC-3'	This study	N/A
Human *ACSS2* primer forward: 5'-CATCAGCTTCTGGTCCAAGTG-3'	This study	N/A
Human *ACSS2* primer reverse: 5'-GCTGGAATCCAAGATCCGTTCAC-3'	This study	N/A
Human *HMGCS1* primer forward: 5'-CTCCCTGACGTGGAATGTCT-3'	This study	N/A

Human *HMGCS1* primer reverse: 5'-GAACTGTCTGCCCAGGTGAT-3'	This study	N/A
Human *HMGCR* primer forward: 5'-GACGTGAACCTATGCTGGTCAG-3'	This study	N/A
Human *HMGCR* primer reverse: 5'-GGTATCTGTTTCAGCCACTAAGG-3'	This study	N/A
Human *MVK* primer forward: 5'-CACCTCAGAGCAAGTGGAGAAG-3'	This study	N/A
Human *MVK* primer reverse: 5'-TGCTGCCAGACACACCGAGTAG-3'	This study	N/A
Human *MVD* primer forward: 5'-CTCGGTGAAGTCCTTGCTGATG-3'	This study	N/A
Human *MVD* primer reverse: 5'-AGCGCGATGAAGAGCTGGTTC-3'	This study	N/A
Human *IDI1* primer forward: 5'-CTCCTGGCAGAGATGTGTATCC-3'	This study	N/A
Human *IDI1* primer reverse: 5'-CGGCTGGATTGCTTAATGGATG-3'	This study	N/A
Human *NSDHL* primer forward: 5'-GGATCGGTGGCTCTGGATTC-3'	This study	N/A
Human *NSDHL* primer reverse: 5'-GCAGAGGTCACCCAGAAAG-3'	This study	N/A
Human *SQLE* primer forward: 5'-CTCCAAGTTCAGGAAAAGCCTGC-3'	This study	N/A
Human *SQLE* primer reverse:	This study	N/A

5’-GAGAACTGGACTCGGGTTAGCT-3’		
Human *CYP51A1* primer forward: 5’-CTCTTACCAGGTTGGCTGCCTT-3’	This study	N/A
Human *CYP51A1*primer reverse: 5’-CTTGAGACTGTCTGCGTTTCTGG-3’	This study	N/A
Human *DHCR7* primer forward: 5’-CAGCGCCAGAGACTGCAAA-3’	This study	N/A
Human *DHCR7* primer reverse: 5’-CAGCTTGAATCAAACCACTTCCC-3’	This study	N/A
Human *FDFT1* primer forward: 5’-TGTGACCTCTGAACAGGAGTGG-3’	This study	N/A
Human *FDFT1* primer reverse: 5’-CCCATAGAGTTGGCACGTTCTG-3’	This study	N/A
Human *LDLR* primer forward: 5’-CACGAAGTCAGGAAGATG-3’	This study	N/A
Human *LDLR* primer reverse: 5’-GGGTGCTGCAGATCATTC-3’	This study	N/A
Human *SREBF2* primer forward: 5’-GCTGCCAAGGAGAGTCTATAC-3’	This study	N/A
Human *SREBF2* primer reverse: 5’-GGCCTGAGGTTTCACCAAG-3’	This study	N/A
Human *SCAP* primer forward: 5’-CAAGAACCTCCTGGCAGTAG-3’	This study	N/A
Human *SCAP* primer reverse: 5’-CATGGAAGCGTTCCCAGTC-3’	This study	N/A

Human *INSIG1* primer forward: 5'-TAGCCCTGGTGCTCAAC-3'	This study	N/A
Human *INSIG1* primer reverse: 5'-AGCACTGGCGTGGTTAATG-3'	This study	N/A
Human *LGALS3* primer forward: 5'-GATGCGTTATCTGGGTCTGG-3'	This study	N/A
Human *LGALS3* primer reverse: 5'-GCACTTGGCTGTCCAGAAGATG-3'	This study	N/A
Human *ABCA1* primer forward: 5'-GATGCGTTATCTGGGTCTGG-3'	This study	N/A
Human *ABCA1* primer reverse: 5'-GCACTTGGCTGTCCAGAAGATG-3'	This study	N/A
Human *ACAT1* primer forward: 5'-CAGTAACAGCTGCCAATGC-3'	This study	N/A
Human *ACAT1* primer reverse: 5'-GGTTCTACAGCAGCGTCAG-3'	This study	N/A
Recombinant DNA		
SCAP shRNA#1	Horizon (Dharmacon)	Cat#V3SH11240_227412984
SCAP shRNA#2	Horizon (Dharmacon)	Cat#V3SH11240_228955440
SCAP shRNA#3	Horizon (Dharmacon)	Cat#V3SH11240_228534848
Insig1 shRNA#1	Horizon (Dharmacon)	Cat#V3SH11240_227321339

Insig1 shRNA#2	Horizon (Dharmacon)	Cat#V3SH11240_228332166
Insig1 shRNA#3	Horizon (Dharmacon)	Cat#V3SH11240_226630552
Non-targeting shRNA	Horizon (Dharmacon)	Cat#VSC11716
pcDNA-EF-Gal3_GFP	This study	
Software and algorithms		
ImageJ		https://imagej.net/ij/
GSEA		https://www.gsea-msigdb.org/gsea/index.jsp
Graphpad Prism	PRISM 10	licensed

616

617 **EXPERIMENTAL MODEL DETAILS**

618 **CELL CULTURE**

619 THP1 and THP1 dual monocytes purchased from ECACC were used in this study. Both THP1
620 and THP1 dual monocytes were cultured in RPMI 1640 containing 10% FBS and 1 mM sodium
621 pyruvate at 37^0C in a 5% CO_2 humidified incubator. They were differentiated into macrophages
622 using 100 nM Phorbol-13-myristate 13-acetate (PMA) for 24 hours, followed by media change.
623 Following a resting period of 48 hours, cells were utilized for respective experiments.

624 **BACTERIAL STRAINS AND MEDIA**

625 Mtb Erdmann strain was grown in Middlebrook 7H9 medium with 4% Albumin-dextrose-saline Or
626 Middlebrook 7H10 plates supplemented with 10% oleic acid-albumin-dextrose-catalase (OADC)
627 at 37^0C. A final concentration of 0.05% Tween 80 was added to the liquid medium.

628 **METHOD DETAILS**

629 **RNA sequencing and analysis:**

630 Total RNA was isolated from the Mtb-infected macrophages after treatment with anti-TB drugs
631 (Isoniazid and rifampicin) in the presence or absence of sertraline for 18 hours. Total RNA was
632 used for stranded library preparation and paired-end clustering with 150bp x 2 end of sequencing
633 performed on HiSeqX (Illumina) by Medgenome Labs. Raw and processed RNA-Seq data are
634 openly available on GEO database (GSE308209). Quality check of raw sequenced reads was
635 performed using Fastqc 0.12.1 and summarized with Multiqc 0.4. Adapters (Illumina universal
636 adapters) and poor-quality bases were trimmed using Trimmomatic 0.39. The trimmed reads were
637 aligned to the human genome gtf (v44) using Star (2.7.10b). Finally, the rawcounts matrix was
638 generated using Subread 2.0.6. Differential gene expression analysis was conducted via
639 edgeR3.42.4. Gene set enrichment analysis was used to compare datasets.

640 **Quantitative PCR:**

641 RNA was isolated using RNAzol (Sigma), and cDNA was synthesized using oligo-dT primers
642 using Verso cDNA synthesis kit following the manufacturer's protocol. Quantitative PCR was
643 performed using KAPA SYBR green (Sigma) on a LightCycler480 (Roche).

644 **Total cholesterol estimation:**

645 THP1 monocytes were seeded in a 24-well plate at a density of 0.5*10^6 cells. Cells after washing
646 with 1X PBS were lysed in 100ul of 1% Triton X-100 for 20 mins on ice. Protein was estimated by
647 the BCA protein estimation kit following the protocol given. For total lipid isolation, 400µL of
648 chloroform: methanol (1:2) was added along with 100µL of 50 mM citric acid. The mix was
649 vortexed and spun down. After the addition of 100µL of autoclaved water, the mix was vortexed
650 and spun down, and finally, 100µL of chloroform was added. After centrifugation of the mix at
651 12000g for 10 minutes, the lower phase was collected and vacuum centrifuged for 30 minutes.
652 The pellet was diluted in cholesterol assay buffer, and total cholesterol levels were assessed

653 using the Total Cholesterol & Cholesteryl Ester Colorimetric Assay Kit (ab282928) following the
654 recommended protocol. Values were normalized with the protein content.

655 **Macrophage infection:**

656 The Mtb culture was centrifuged and washed with PBST (1x PBS with 0.05% of Tween 80) twice,
657 and a single cell suspension was made after spinning down the culture at 800g for 10 minutes.
658 THP1 dual macrophages were infected for 6 hours at MOI5. After 6 hours, cells were washed
659 twice with 1X PBS, and appropriate cell culture media was added.

660 **Intracellular bacterial growth assay:**

661 THP1 dual monocytes were seeded in a 48-well plate at a density of 0.15 million cells. Cells were
662 differentiated into macrophages as indicated, and after a 48-hour resting period, cells were
663 infected with Mtb for 6 hours at MOI5. After stopping the infection, cells were treated with drugs
664 isoniazid (20ng/mL), rifampicin (100ng/mL), and sertraline (20μM) given in 10% FBS RPMI media.
665 At day 3 post-treatment, cells were lysed with water containing 0.05% Tween 80, and dilutions of
666 intracellular bacteria were made in PBST. The final diluted lysate was plated on 7H10 plates.
667 To restrict cholesterol uptake by the macrophages, treatment with TB drugs was given in RPMI
668 media supplemented with 10% Lipoprotein-deficient serum (LPDS).
669 For the cholesterol replenishment assay, Mtb-infected THP1 macrophages were treated with
670 cholesterol (2μg/ml) for an hour after infection, followed by incubation with anti-TB drugs in LPDS
671 medium, and further cholesterol was added every 24 hours.

672 **Immunoblotting**

673 THP1 dual macrophages were lysed in RIPA buffer along with a protease inhibitor cocktail.
674 Protein concentration was estimated by BCA assay, and 50μg of total protein was loaded per
675 sample in a 10% polyacrylamide gel. Protein was transferred to a nitrocellulose membrane, and
676 the membrane was blocked using a 5% BSA solution. The membrane was next incubated
677 overnight in anti-rabbit SREBP2 antibody, on shaking at 4°C. Next, the membrane was washed
678 thrice with PBST (1X PBS with 0.05% Tween 20) solution and incubated with HRP-conjugated

679 secondary antibody for an hour at room temperature. After washing with PBST, the membrane
680 was imaged using ImageQuant LAS 500. The protein markers used are Prestained Protein ladder
681 (MBT092) and puregene three color prestained protein ladder (PG- PMT2922).

682 **Filipin Staining:**

683 The THP1 macrophages were seeded in confocal chamber slides (1.5*10^4 cells per chamber)
684 and treated with sertraline at 20μM for 24 hours. Cells were washed twice with 1x PBS before
685 fixation with 4% methanol-free formaldehyde in 1X PHEM buffer for 20 mins at room temperature.
686 After an additional wash with 1x PBS, cells were stained with filipin staining solution (50ug/ml
687 diluted in 1x PBS) for an hour in the dark at room temperature. Next, the cells were washed with
688 1x PBS and imaged on a Leica SP8 laser scanning confocal microscope. Filipin was excited at
689 the 405nm laser.

690 **Cholesterol compartmentalization assay:**

691 THP1 monocytes were seeded at a density of 0.15 million cells in a four-chamber confocal dish
692 and differentiated as mentioned. The NBD-cholesterol at a final conc of 10μM was added for 24
693 hours along with the different compounds such as sertraline (20μM), citalopram (20μM), and
694 U18666A (2.5μg/ml). Before initiation of imaging, cells were stained with Lysotracker Red
695 (100nM) along with Hoechst dye for 1 hour in 10% FBS containing RPMI. Images were taken
696 using a Leica SP8 laser scanning confocal microscope.

697 **Stable knockdown/overexpression cell line generation:**

698 Lenti-X 293T cells were transfected with pVSVG and pDR8.2 plasmids together with lentiviral
699 constructs expressing gene-specific shRNA or non-targeting controls to generate viral particles.
700 After 6 hours of transfection, the media was changed to 2% FBS containing DMEM, and after 48
701 hours, the cell supernatant was collected and centrifuged at 100g for 5 minutes to remove cell
702 debris. Further, this supernatant was filtered through a 0.45μ syringe filter, and viral particles were
703 concentrated using a 30kDa centricon filter. For transduction in THP1 monocytes, 50,000 cells
704 were seeded in a 24-well plate, and 100μL of viral stock was added along with a final

705 concentration of 8μg/mL polybrene. After 24 hours media was changed, and antibiotic selection
706 was initiated after 48 hours of transduction with 0.6μg/mL of puromycin. Cells showing tRFP
707 fluorescence co-expressed with shRNA were checked regularly.
708 The hGal3 and eGFP are excised from the pEGFP-hGal3 plasmid using Nhe1, Nde1, and Msc1
709 restriction enzymes and ligated to Xba1 and Msc1 digested pcDNA 3.1 vector. The final plasmid
710 is transfected into THP1 monocytes using Lipofectamine LTX.
711 **Computational assessment of NPC1- SSRI interactions:**
712 A composite structure of NPC- 1 protein (cryo-EM, PDB IDL 6W5V) with the addition of missing
713 atoms (PDB Fixer) (61) and validated for structure quality by Procheck (62) for Ramachandran
714 parameters were used as a template for the analysis of interaction with SSRIs- Sertraline and
715 citalopram. Ligand structures of Cholesterol, U18666A, sertraline, and citalopram from the PDB
716 ligand library were converted from SDF to PDB format using OpenBabel (63)and used for docking
717 studies focused on the binding region reported earlier (23). The residues reported to interact with
718 sertraline were selected as the binding site region, with the centroid of the binding site used as
719 the center of the grid box with dimensions (40,40,40 npts) for docking analysis with 50 iterations
720 for each ligand by Autodock4.2 (64). The docked poses were clustered at the default value of
721 2.0Å RMSD, and the clusters were ranked based on the lowest binding energy in each cluster.
722 The binding energy is calculated in AutoDock as a semi-empirical function of intermolecular forces
723 such as Vanderwaals forces, hydrogen bonds, desolvation energy, electrostatic energy, and
724 torsional energies (65). The binding energy of the best docked pose, the mean binding energy of
725 the top cluster, and the total number of clusters were noted. The docked pose with the lowest
726 binding energy was visualised using PyMOL, and the protein-ligand interactions were predicted
727 using PLIP (66).
728 **Galectin 3 puncta assessment:**
729 GFP tagged galectin-3 overexpressing THP1 monocytes were seeded in a chambered confocal
730 dish and treated with sertraline (20μM) and citalopram (20μM) for 24 hours, and with 1mM LLOMe

731 for 15 minutes. Before imaging, cells were stained with Lyostracker Red and Hoechst for an hour.
732 Images were taken using a Leica SP8 laser scanning confocal microscope.

733 **Mitochondrial ROS estimation:**

734 THP1 dual cells were differentiated as indicated. Treatment was given with rotenone at 10μM for
735 30 minutes or with different indicated compounds. The cells were incubated with 5μM of MitoSox
736 dye for 30 minutes. After washing with 1X PBS, cells were imaged in the Invitrogen™ EVOS™
737 M5000 Imaging System.

738 **ELISA:**

739 THP1 dual macrophages were infected with Mtb at MOI5 and treated with different compounds.
740 Supernatant was collected at the indicated time points and filtered through a 0.2μ filter.
741 Concentration of IL-1β was determined using an ELISA kit following the recommended protocol.

742 **Statistical analysis**

743 The results are depicted as mean ± SEM. Statistical analysis was carried out using Student's t-
744 test (Welch's test or Mann-Whitney test) using GraphPad Prism. P values less than 0.05, 0.01,
745 0.005 are represented as *, ** and *** respectively.

746

747 **References:**

748 1. J. Chakaya *et al.*, The WHO Global Tuberculosis 2021 Report - not so good news and
749 turning the tide back to End TB. *Int J Infect Dis* **124 Suppl 1**, S26-S29 (2022).
750 2. Anonymous, Global tuberculosis report 2024. (2024).
751 3. A. Trajman *et al.*, Tuberculosis. *Lancet* **405**, 850-866 (2025).
752 4. E. H. Tobin, D. Tristram, "Tuberculosis Overview" in StatPearls. (Treasure Island (FL),
753 2025).
754 5. A. Matteelli, S. Lovatti, B. Rossi, L. Rossi, Update on multidrug-resistant tuberculosis
755 preventive therapy toward the global tuberculosis elimination. *Int J Infect Dis* **155**,
756 107849 (2025).
757 6. P. Nahid *et al.*, Treatment of Drug-Resistant Tuberculosis. An Official
758 ATS/CDC/ERS/IDSA Clinical Practice Guideline. *Am J Respir Crit Care Med* **200**, e93-
759 e142 (2019).
760 7. C. Young, G. Walzl, N. Du Plessis, Therapeutic host-directed strategies to improve
761 outcome in tuberculosis. *Mucosal Immunol* **13**, 190-204 (2020).
762 8. E. B. Wong, K. A. Cohen, W. R. Bishai, Rising to the challenge: new therapies for
763 tuberculosis. *Trends Microbiol* **21**, 493-501 (2013).

764 9. D. Shankaran *et al.*, The antidepressant sertraline provides a novel host directed therapy
765 module for augmenting TB therapy. *Elife* **12** (2023).
766 10. A. Singh, K. Bisht, N. Yadav, R. Nanda, V. Rao, Inflammasome activation dictates the
767 efficacy of antimycobacterial activity of frontline TB drugs. *bioRxiv*
768 10.1101/2025.04.02.646750, 2025.2004.2002.646750 (2025).
769 11. R. J. King, P. K. Singh, K. Mehla, The cholesterol pathway: impact on immunity and
770 cancer. *Trends Immunol* **43**, 78-92 (2022).
771 12. A. Canfran-Duque *et al.*, Macrophage-Derived 25-Hydroxycholesterol Promotes
772 Vascular Inflammation, Atherogenesis, and Lesion Remodeling. *Circulation* **147**, 388-
773 408 (2023).
774 13. A. Reboldi, E. Dang, Cholesterol metabolism in innate and adaptive response.
775 *F1000Res* **7** (2018).
776 14. F. A. de Freitas *et al.*, Effects of Oxysterols on Immune Cells and Related Diseases.
777 *Cells* **11** (2022).
778 15. J. G. Cyster, E. V. Dang, A. Reboldi, T. Yi, 25-Hydroxycholesterols in innate and
779 adaptive immunity. *Nat Rev Immunol* **14**, 731-743 (2014).
780 16. P. Duewell *et al.*, NLRP3 inflammasomes are required for atherogenesis and activated
781 by cholesterol crystals. *Nature* **464**, 1357-1361 (2010).
782 17. M. Schonewille *et al.*, Statins increase hepatic cholesterol synthesis and stimulate fecal
783 cholesterol elimination in mice. *J Lipid Res* **57**, 1455-1464 (2016).
784 18. L. Chen *et al.*, Cholesterol-rich lysosomes induced by respiratory syncytial virus promote
785 viral replication by blocking autophagy flux. *Nat Commun* **15**, 6311 (2024).
786 19. W. Eid *et al.*, mTORC1 activates SREBP-2 by suppressing cholesterol trafficking to
787 lysosomes in mammalian cells. *Proc Natl Acad Sci U S A* **114**, 7999-8004 (2017).
788 20. A. Radhakrishnan, Y. Ikeda, H. J. Kwon, M. S. Brown, J. L. Goldstein, Sterol-regulated
789 transport of SREBPs from endoplasmic reticulum to Golgi: oxysterols block transport by
790 binding to Insig. *Proc Natl Acad Sci U S A* **104**, 6511-6518 (2007).
791 21. A. Frolov *et al.*, NPC1 and NPC2 regulate cellular cholesterol homeostasis through
792 generation of low density lipoprotein cholesterol-derived oxysterols. *J Biol Chem* **278**,
793 25517-25525 (2003).
794 22. K. B. Peake, J. E. Vance, Defective cholesterol trafficking in Niemann-Pick C-deficient
795 cells. *FEBS Lett* **584**, 2731-2739 (2010).
796 23. K. Alvarez-Valadez *et al.*, Lysosomal damage due to cholesterol accumulation triggers
797 immunogenic cell death. *Autophagy* **21**, 934-956 (2025).
798 24. R. A. DeBose-Boyd *et al.*, Transport-dependent proteolysis of SREBP: relocation of site-
799 1 protease from Golgi to ER obviates the need for SREBP transport to Golgi. *Cell* **99**,
800 703-712 (1999).
801 25. P. Hu *et al.*, Cholesterol-associated lysosomal disorder triggers cell death of
802 hematological malignancy: Dynamic analysis on cytotoxic effects of LW-218. *Acta*
803 *Pharm Sin B* **11**, 3178-3192 (2021).
804 26. S. Aits *et al.*, Sensitive detection of lysosomal membrane permeabilization by lysosomal
805 galectin puncta assay. *Autophagy* **11**, 1408-1424 (2015).
806 27. D. L. Thiele, P. E. Lipsky, The action of leucyl-leucine methyl ester on cytotoxic
807 lymphocytes requires uptake by a novel dipeptide-specific facilitated transport system
808 and dipeptidyl peptidase I-mediated conversion to membranolytic products. *J Exp Med*
809 **172**, 183-194 (1990).
810 28. O. B. Davis *et al.*, NPC1-mTORC1 Signaling Couples Cholesterol Sensing to Organelle
811 Homeostasis and Is a Targetable Pathway in Niemann-Pick Type C. *Dev Cell* **56**, 260-
812 276 e267 (2021).
813 29. L. A. Martin, B. E. Kennedy, B. Karten, Mitochondrial cholesterol: mechanisms of import
814 and effects on mitochondrial function. *J Bioenerg Biomembr* **48**, 137-151 (2016).

30. M. de la Mata *et al.*, Mitochondrial Dysfunction in Lysosomal Storage Disorders. *Diseases* **4** (2016).
31. L. Goicoechea, L. Conde de la Rosa, S. Torres, C. Garcia-Ruiz, J. C. Fernandez-Checa, Mitochondrial cholesterol: Metabolism and impact on redox biology and disease. *Redox Biol* **61**, 102643 (2023).
32. E. Balboa *et al.*, MLN64 induces mitochondrial dysfunction associated with increased mitochondrial cholesterol content. *Redox Biol* **12**, 274-284 (2017).
33. J. X. Lin *et al.*, Rab7a-mTORC1 signaling-mediated cholesterol trafficking from the lysosome to mitochondria ameliorates hepatic lipotoxicity induced by aflatoxin B1 exposure. *Chemosphere* **320**, 138071 (2023).
34. M. Mari, A. Morales, A. Colell, C. Garcia-Ruiz, J. C. Fernandez-Checa, Mitochondrial glutathione, a key survival antioxidant. *Antioxid Redox Signal* **11**, 2685-2700 (2009).
35. C. Guo *et al.*, Cholesterol Homeostatic Regulator SCAP-SREBP2 Integrates NLRP3 Inflammasome Activation and Cholesterol Biosynthetic Signaling in Macrophages. *Immunity* **49**, 842-856 e847 (2018).
36. T. Hu *et al.*, Metabolic regulation of the immune system in health and diseases: mechanisms and interventions. *Signal Transduct Target Ther* **9**, 268 (2024).
37. M. Andersson *et al.*, Pharmacokinetics of intra-arterial mitomycin C with or without degradable starch microspheres (DSM) in the treatment of non-resectable liver cancer. *Acta Oncol* **28**, 219-222 (1989).
38. T. O. Omotade, C. R. Roy, Manipulation of Host Cell Organelles by Intracellular Pathogens. *Microbiol Spectr* **7** (2019).
39. T. M. Clemente, R. K. Angara, S. D. Gilk, Establishing the intracellular niche of obligate intracellular vacuolar pathogens. *Front Cell Infect Microbiol* **13**, 1206037 (2023).
40. C. Perez-Guzman, M. H. Vargas, Hypocholesterolemia: a major risk factor for developing pulmonary tuberculosis? *Med Hypotheses* **66**, 1227-1230 (2006).
41. Y. S. Jo *et al.*, Relationship between total cholesterol level and tuberculosis risk in a nationwide longitudinal cohort. *Sci Rep* **11**, 16254 (2021).
42. V. Chidambaram *et al.*, Higher Serum Cholesterol Levels Are Associated With Reduced Systemic Inflammation and Mortality During Tuberculosis Treatment Independent of Body Mass Index. *Front Cardiovasc Med* **8**, 696517 (2021).
43. A. Parivakkam Mani, S. K, D. K. K, S. Yadav, Assessment of Lipid Profile in Patients With Pulmonary Tuberculosis: An Observational Study. *Cureus* **15**, e39244 (2023).
44. S. Y. Bah, P. Dickinson, T. Forster, B. Kampmann, P. Ghazal, Immune oxysterols: Role in mycobacterial infection and inflammation. *J Steroid Biochem Mol Biol* **169**, 152-163 (2017).
45. S. Hayakawa *et al.*, Activated cholesterol metabolism is integral for innate macrophage responses by amplifying Myd88 signaling. *JCI Insight* **7** (2022).
46. E. S. Istvan, J. Deisenhofer, Structural mechanism for statin inhibition of HMG-CoA reductase. *Science* **292**, 1160-1164 (2001).
47. J. F. Xu *et al.*, Statins and pulmonary fibrosis: the potential role of NLRP3 inflammasome activation. *Am J Respir Crit Care Med* **185**, 547-556 (2012).
48. B. D. Henriksbo *et al.*, Fluvastatin causes NLRP3 inflammasome-mediated adipose insulin resistance. *Diabetes* **63**, 3742-3747 (2014).
49. A. Altaf *et al.*, NLRP3 inflammasome in peripheral blood monocytes of acute coronary syndrome patients and its relationship with statins. *Coron Artery Dis* **26**, 409-421 (2015).
50. D. Ebrahimi-Fakhari *et al.*, Reduction of TMEM97 increases NPC1 protein levels and restores cholesterol trafficking in Niemann-pick type C1 disease cells. *Hum Mol Genet* **25**, 3588-3599 (2016).
51. T. Nishimura *et al.*, Inhibition of cholesterol biosynthesis by 25-hydroxycholesterol is independent of OSBP. *Genes Cells* **10**, 793-801 (2005).

52. H. Choi *et al.*, 25-Hydroxycholesterol modulates microglial function and exacerbates Alzheimer's disease pathology: mechanistic insights and therapeutic potential of cholesterol esterification inhibition. *J Neuroinflammation* **22**, 50 (2025).
53. W. J. Griffiths, Y. Wang, Cholesterol metabolism: from lipidomics to immunology. *J Lipid Res* **63**, 100165 (2022).
54. A. Reboldi *et al.*, Inflammation. 25-Hydroxycholesterol suppresses interleukin-1-driven inflammation downstream of type I interferon. *Science* **345**, 679-684 (2014).
55. M. Viaud *et al.*, Lysosomal Cholesterol Hydrolysis Couples Efferocytosis to Anti-Inflammatory Oxysterol Production. *Circ Res* **122**, 1369-1384 (2018).
56. R. Zhou, A. S. Yazdi, P. Menu, J. Tschopp, A role for mitochondria in NLRP3 inflammasome activation. *Nature* **469**, 221-225 (2011).
57. S. Leishman *et al.*, Fatty acid synthesis promotes inflammasome activation through NLRP3 palmitoylation. *Cell Rep* **43**, 114516 (2024).
58. O. F. Kuzu, M. Toprak, M. A. Noory, G. P. Robertson, Effect of lysosomotropic molecules on cellular homeostasis. *Pharmacol Res* **117**, 177-184 (2017).
59. J. M. Albright, A. Holian, Contribution of particle-induced lysosome membrane permeabilization to NLRP3 inflammasome activation and mitochondrial ROS production. *Toxicol Sci* **208**, 357-368 (2025).
60. C. Bussi *et al.*, Lysosomal damage drives mitochondrial proteome remodelling and reprograms macrophage immunometabolism. *Nat Commun* **13**, 7338 (2022).
61. P. Eastman *et al.*, OpenMM 7: Rapid development of high performance algorithms for molecular dynamics. *PLoS Comput Biol* **13**, e1005659 (2017).
62. R. A. Laskowski, J. A. Rullmannn, M. W. MacArthur, R. Kaptein, J. M. Thornton, AQUA and PROCHECK-NMR: programs for checking the quality of protein structures solved by NMR. *J Biomol NMR* **8**, 477-486 (1996).
63. N. M. O'Boyle *et al.*, Open Babel: An open chemical toolbox. *J Cheminform* **3**, 33 (2011).
64. G. M. Morris *et al.*, AutoDock4 and AutoDockTools4: Automated docking with selective receptor flexibility. *J Comput Chem* **30**, 2785-2791 (2009).
65. R. Huey, G. M. Morris, A. J. Olson, D. S. Goodsell, A semiempirical free energy force field with charge-based desolvation. *J Comput Chem* **28**, 1145-1152 (2007).
66. S. Salentin, S. Schreiber, V. J. Haupt, M. F. Adasme, M. Schroeder, PLIP: fully automated protein-ligand interaction profiler. *Nucleic Acids Res* **43**, W443-447 (2015).